High Power Laser Science and Engineering, (2016), Vol. 4, e45, 8 pages.

doi:10.1017/hpl.2016.44

Accelerating ions with high-energy short laser pulses from submicrometer thick targets

F. Wagner[1,2], C. Brabetz[1], O. Deppert[3], M. Roth[3], T. Stöhlker[1,2], An. Tauschwitz[4], A. Tebartz[3], B. Zielbauer[1], and V. Bagnoud[1,2]

[1]*GSI Helmholtzzentrum für Schwerionenforschung GmbH, Planckstraße 1, 64291 Darmstadt, Germany*

[2]*Helmholtz Institut Jena, Fröbelstieg 3, 07743 Jena, Germany*

[3]*Institut für Kernphysik, Technische Universität Darmstadt, Schlossgartenstraße 9, 64289 Darmstadt, Germany*

[4]*Institute for Theoretical Physics, Frankfurt University, Max-von-Laue-Str. 1, 60438 Frankfurt am Main, Germany*

(Received 24 June 2016; revised 1 October 2016; accepted 25 October 2016)

Abstract

Using the example of the PHELIX high-energy short pulse laser we discuss the technical preconditions to investigate ion acceleration with submicrometer thick targets. We show how the temporal contrast of this system was improved to prevent pre-ionization of such targets on the nanosecond timescale. Furthermore the influence of typical fluctuations or uncertainties of the on-target intensity on ion acceleration experiments is discussed. We report how these uncertainties were reduced by improving the assessment and control of the on-shot intensity and by optimizing the positioning of the target into the focal plane. Finally we report on experimental results showing maximum proton energies in excess of 85 MeV for ion acceleration via the target normal sheath acceleration mechanism using target thicknesses on the order of one micrometer.

Keywords: high-power laser technique; laser-ion acceleration; relativistic laser plasma interaction; target normal sheath acceleration; temporal contrast

1. Introduction: Laser-driven ion acceleration using ultrathin targets

Laser-driven ion acceleration is an important application of high-power laser facilities. One of the main goals is to increase the conversion efficiency from laser energy to the accelerated ions and in doing so increase the particle flux and maximum ion energy. This is particularly important for several proposed applications, e.g., medical treatment[1], generation of energetic neutron beams[2] and fast ignition in the frame of inertial confinement fusion[3].

With the technological progress regarding temporal contrast of ultraintense laser pulses in recent years, the use of submicrometer thick targets has become possible. Several investigations have shown that the energy maximum of ions accelerated via the target normal sheath acceleration (TNSA) mechanism[4] can be enhanced significantly by using target thicknesses which are small compared to the focal spot diameter[5–7]. At the same time, alternative mechanisms based on the use of submicrometer thick targets and ultrahigh intensities ($>10^{20}$ W cm^{-2}) have been proposed aiming at increased maximum ion energy and conversion efficiency: laser breakout afterburner (BOA)[8] and radiation pressure acceleration (RPA)[9].

Furthermore, the achievable ion energy can be enhanced by increasing the on-target intensity. This problem has two aspects: First, raising the intensity of the fully amplified and focussed laser pulse, and second, positioning the target into the plane of maximum intensity. For a given pulse duration and energy, the accessible intensity is preassigned by the focussing capability of such pulses to the smallest spotsize which is limited by the beam quality. Especially high-energy Nd:glass laser systems suffer from strong beam aberrations because of the large used optics and the poor thermal properties of glass. Such aberrations are complicated to handle and besides restraining the intensity they also add an uncertainty to the assessment of the achieved intensity which is an issue for the interpretation of experimental results.

In this paper, we discuss the technical preconditions to investigate ion acceleration with ultrathin targets using the example of the PHELIX (Petawatt High Energy

Correspondence to: F. Wagner, GSI Helmholtzzentrum für Schwerionenforschung GmbH, Planckstraße 1, 64291 Darmstadt, Germany. Email: f.wagner@gsi.de

Laser for heavy Ion eXperiments) laser facility[10] at GSI Helmholtzzentrum für Schwerionenforschung GmbH in Darmstadt, Germany. We also discuss our recent experimental observation of maximum proton energies in excess of 85 MeV by laser-driven ion acceleration via the TNSA mechanism[11].

2. Temporal contrast issues

The use of ultrathin targets imposes high demands on the temporal qualities of the laser pulse. An important figure of merit is the temporal contrast, defined by the ratio of the peak intensity to the intensity at a given time before this maximum. This quality has a major effect on laser-driven ion acceleration. At a given intensity level preceding the peak, pre-ionization occurs, leading to an expanded preplasma at the target surface[12]. While for sufficiently thick targets this could even be beneficial since self-focussing and enhanced absorption in the preplasma cloud might increase the effective intensity, this is an issue for very thin targets. An ultrathin target can be turned into an underdense plasma which precludes the above mentioned mechanisms for laser-driven ion acceleration.

For TNSA it has been shown that an undisturbed rear target surface is strongly favorable since an extended plasma density would attenuate the accelerating field, decreasing the maximum achievable ion energy. Therefore, the intensity preceding the peak must stay below a certain value which depends on the target thickness[13].

The effect of preplasma expansion on the BOA mechanism has not been studied extensively yet. However, the theoretical description of this mechanism implies a classically overdense target which becomes relativistically transparent while interacting with the peak laser intensity[8]. This is in accordance with the experimental observation of an optimum target thickness[14]. While for a target that is much thicker than this optimum, relativistic transparency is not achieved, a considerably thinner target becomes classically underdense long before the impact of the pulse maximum. This is strongly influenced by the temporal contrast since a substantial preplasma expansion could turn the target into an underdense plasma which would frustrate the BOA mechanism.

The theoretical model of the RPA mechanism is fundamentally different from the BOA mechanism. An ultrathin target (∼10 nm) must stay opaque during the interaction which poses even higher demands on the temporal contrast of the laser pulse compared to BOA.

To summarize the investigation of ion acceleration with ultrathin targets requires sufficient control over the temporal contrast. However, the amplification of short laser pulses via the chirped pulse amplification (CPA) scheme leads to a major degradation of the temporal contrast. The amplified pulse has a complicated structure including a pedestal of amplified spontaneous emission (ASE), compressed prepulses as well as a slope which rises slowly compared to an ideal Gaussian pulse[15]. The latter is also identified as coherent pedestal. An example is given in Figure 1, showing a temporal profile of the PHELIX short pulse measured in 2010.

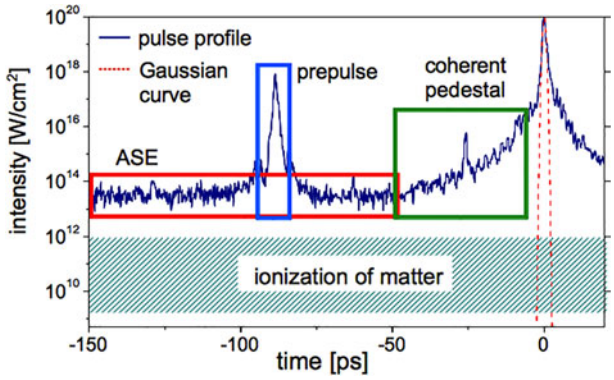

Figure 1. Temporal profile of the PHELIX pulse in 2010 before the application of pulse cleaning techniques, measured with a third order cross-correlator (Sequoia, Amplitude Technologies). The curve has been scaled to a peak intensity of 10^{20} W cm^{-2}. The shaded area illustrates the ionization threshold for typical target materials. The red dashed line shows a Gaussian function with the same FWHM as the pulse (blue).

The effect of the temporal contrast on the nanosecond timescale on the target conditions can be modeled using hydrodynamic simulation codes. As an example, Figure 2 shows the results of two simulations carried out with the 2-dimensional radiation hydrodynamics code RALEF-2D (Radiation Arbitrary Lagrangian–Eulerian Fluid dynamics)[16]. The graph shows lineouts of the electron density of initially 4 μm thick copper targets irradiated with a linearly growing intensity for 1 ns followed by a constant plateau lasting 1.5 ns. This temporal structure is a simplified model for the ASE of the PHELIX short pulse. The results of two simulations are shown for two different intensities of the ASE plateau. The higher level of 5×10^{13} W cm^{-2} is a typical value for CPA systems that do not apply contrast improving techniques and peak intensities around 10^{20} W cm^{-2}. A reduction of this level to the lower level of 3×10^{10} W cm^{-2} is usually achievable with modern pulse cleaning techniques as described below. A more detailed description of the simulation setup is given in Ref. [12].

This example shows that for the standard temporal contrast of high-power lasers the target conditions are strongly affected by the ASE. An expanding preplasma forms at the target surface ranging over tens of micrometers. Furthermore the density of an initially 4 μm thick target drops below the critical density. In contrast for the lower ASE level the preplasma dimension is significantly reduced and the initial target shape is preserved to some degree.

In order to decrease the intensity of ASE and prepulses to a value below the ionization threshold of matter, most of

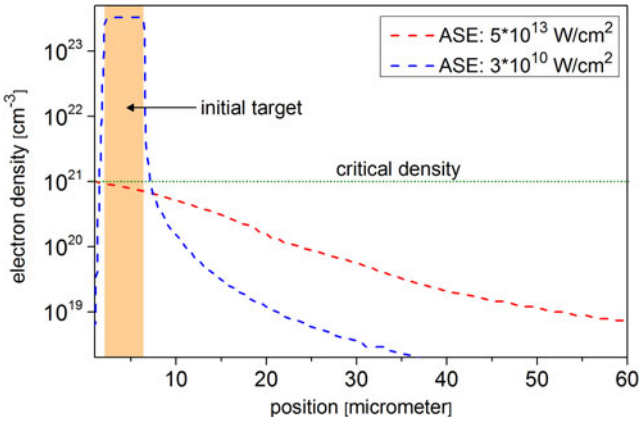

Figure 2. Simulated electron density for two different ASE levels.

the high-power laser facilities have recently started to apply pulse cleaning techniques. It was demonstrated by Itatani[17] that the ASE pedestal can be decreased by increasing the seeding energy of the amplifiers. A common method to generate a suitable seed pulse is the so-called double CPA technique[18]: the oscillator pulse is first amplified to the millijoule level in a CPA stage and subsequently temporally cleaned using one of several nonlinear cleaning techniques, e.g., cross polarized wave[19], saturable absorbers[20] or low gain optical parametric amplification[21]. A second CPA stage is then used to further amplify the pulse to its maximum energy. At the PHELIX system we apply another technique first proposed by Dorrer[22]. The high-energy seed pulse is generated by directly amplifying the short pulse from the oscillator using an ultrafast optical parametric amplifier (uOPA)[15].

3. Meeting the temporal contrast requirements

A schematic of the PHELIX short pulse system is shown in Figure 3. The short (100 fs FWHM) pulses from the oscillator (Mira 900, Coherent) are directly amplified by an uOPA which provides a gain of up to 10^5[15]. Any degradation of the nanosecond and picosecond temporal contrast is precluded by using a dedicated laser-diode pumped pump laser with a pulse duration of about 1 ps[23]. This amplified pulse is then used as a clean seed pulse for the PHELIX CPA system. Consequently the ASE contrast is enhanced proportional to the uOPA gain from a value around 10^6 without the uOPA (compare Figure 1) to an optimum of 10^{11}. The PHELIX CPA system applies two regenerative Ti:sapphire amplifiers and Nd:glass pre- and main amplifiers to provide a maximum energy up to 250 J with a minimum pulse duration of 500 fs. Peak intensities between 10^{20} and 10^{21} W cm^{-2} are achieved by focussing these pulses. Thus the ASE intensity is less than 10^{10} W cm^{-2} which is below the ionization threshold of most of the targets such as CH_2 foils.

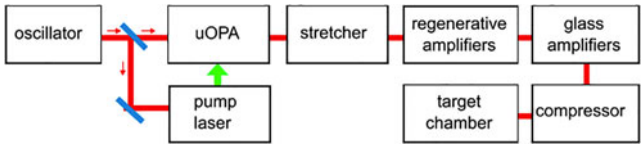

Figure 3. Schematic of the PHELIX short pulse beamline.

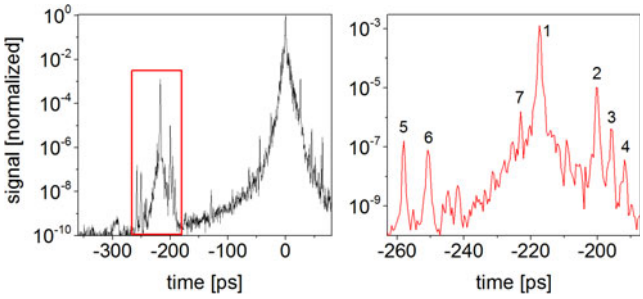

Figure 4. Temporal profile of the PHELIX pulse in 2012 using the uOPA with a gain of 10^4. The pulse was measured with a third order cross-correlator (Sequoia, Amplitude Technologies). The right graph shows an enlargement of the red framed region of the left graph.

Prepulses are generated independently from the ASE mostly after the uOPA stage and therefore have to be treated separately. In CPA systems, the most common origin of prepulses on the picosecond timescale is an interplay between the generation of postpulses due to double reflections from parallel surfaces and the nonlinear Kerr effect[24]. Therefore, the temporal separation between the prepulse and the peak is defined by the optical path difference which allows for identification of the optical element responsible for the prepulse. Figure 4 shows a contrast measurement directly after the implementation of the uOPA at the PHELIX system in 2012. The ASE level is 10 orders of magnitude below the maximum which was the detection limit of that measurement. This measurement revealed several prepulses. Most of these prepulses are in the temporal range between 190 and 270 ps before the peak. Assuming a refractive index of 1.5 this corresponds to optical elements with thicknesses of (1.9–2.7) cm. We could attribute pulses with the numbers 1–3 in the right graph of Figure 4 to Pockels cells with parallel surfaces in the regenerative amplifiers. By switching to specially designed Pockels cells with wedged surfaces these prepulses could be removed. The pulses 5 and 6 could be removed by exchanging two cube polarizers for thin film polarizers. Prepulse 7 was caused by injection of another pulse from the 72 MHz oscillator into the regenerative amplifiers. Therefore, it drops down with increasing gain in the uOPA and can be further diminished by careful adjustment of a Pockels cell pulse picker between the oscillator and the regenerative amplifiers. Though we could not identify the origin of prepulse 4 it is not present anymore in recent measurements.

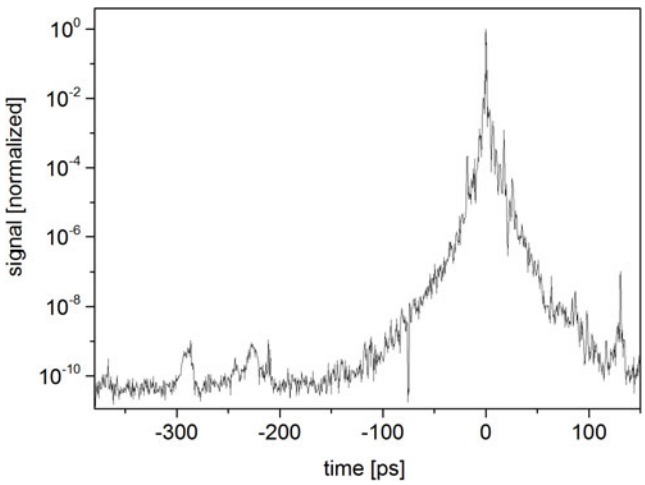

Figure 5. Temporal profile of the PHELIX pulse in November 2015 using the uOPA with a gain of 10^5. The pulse was measured with a third order cross-correlator (Sequoia, Amplitude Technologies).

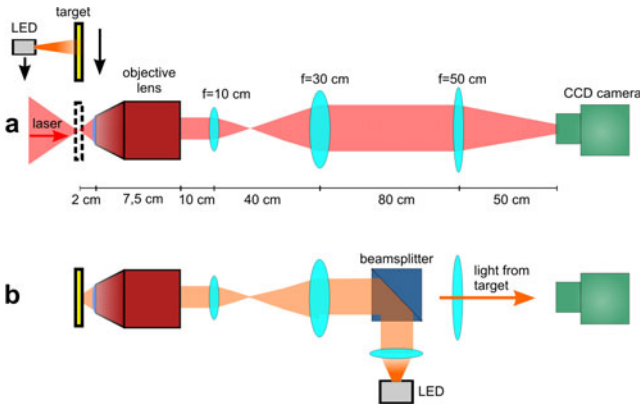

Figure 6. Schematical setup of the focus and target alignment system. (a) The laser focus is imaged on the camera while the target is moved to the side. A transparent target is mapped on the camera by transmitting the light from the LED inside the target chamber through the target. (b) For alignment of opaque targets the LED light is coupled into the diagnostics beamline using a beamsplitter cube and light coming back from the target is imaged onto the camera.

A recent measurement of the temporal contrast on the picosecond timescale is shown in Figure 5. The ASE level is below the detection threshold around 10^{-10}. As we described in Ref. [25] a minimum ASE level around 10^{-11} can be estimated. There are still some minor prepulses which have not been identified yet. However, with a contrast ratio of better than 10^9 they do not reach the ionization threshold of most of the target materials.

Any degradation of the nanosecond contrast, e.g., due to prepulses from the regenerative amplifiers, is prevented by using four isolation stages based on Pockels cells and polarizers. The nanosecond temporal contrast is monitored on a full energy shot by a photodiode capable to detect prepulses with a contrast ratio of 10^{-6} or lower. In addition a high dynamic range (>10 orders of magnitude) measurement of the nanosecond contrast was accomplished using a specially designed cross-correlator which will be described in Ref. [26].

4. Target and focus alignment

To enable peak intensities in excess of 10^{20} W cm^{-2} for laser-ion acceleration experiments, the fully amplified and temporally compressed pulses are typically focussed very tightly using focussing geometries with f-numbers of three or less. To ensure the maximum on-target intensity and to guarantee reproducible experimental conditions, the alignment of the focus and the positioning of the target into the plane of focus is extremely crucial. In practice this means that a positioning accuracy of better than the Rayleigh range of the focussed beam must be accomplished.

At the PHELIX facility we use a specially designed diagnostics system which is schematically shown in Figure 6. The laser pulse is focussed with an f/1.7 focussing parabola inside the PHELIX target chamber. For the optimization of the focal spot, a pulse that is amplified to the millijoule level by the regenerative amplifiers of the PHELIX frontend operating at a repetition rate of 10 Hz is used, while the main glass amplifiers stay passive. The focussed beam is collimated by an objective lens (20× Mitutoyo Plan Apo NIR Infinity Corrected Objective). In combination with a spherical lens a ten-fold enlarged intermediate image of the focus is generated. This intermediate image is then mapped to a camera outside the vacuum chamber with an additional magnification of 1.7. The total magnification of 17 is a reasonable compromise between a sufficiently large field of view to image the target and enough enlargement of the focus to resolve the minimum spot diameter with a standard CCD camera (Basler A622f, pixel size: 7 µm). The numerical aperture (NA) of this imaging system which is defined by the objective lens ($NA_{obj} = 0.4$) is sufficient to catch the whole beam ($NA_{laser} = 0.3$). After focus adjustment, the same imaging system is used to place the target into the focal plane. Therefore, the target is illuminated with an LED (Thorlabs, LED1050E) with a central wavelength of 1050 nm. Using the same wavelength for target illumination as the laser wavelength prevents a shift of the focal plane between focal spot and target alignment due to chromatic aberrations. The target positioning along the focussing direction requires an accuracy better than the Rayleigh range of the laser beam to guarantee a high intensity on the target surface. For the f/1.7 focussing system and a central wavelength of 1053 nm the theoretical minimum waist size is $\omega_0 = 1.2$ µm and the corresponding Rayleigh range equals $z_r = 4$ µm. However, due to a non-ideal beam quality, the realized minimum waist size and the Rayleigh range are $\omega_0 = 3.4$ µm and $z_r = 11$ µm, respectively. Experimentally we achieve a positioning accuracy of about 5 µm which

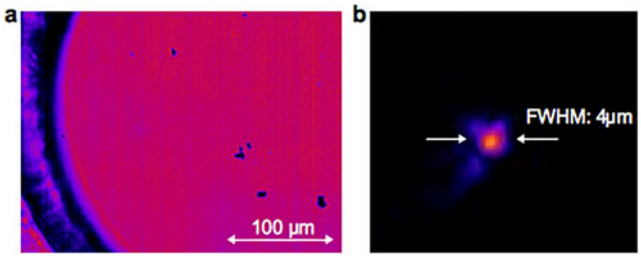

Figure 7. (a) Image of a micrometer thick plastic target attached to a thicker supporting foil with a free aperture of 1 mm. (b) Image of the focal spot.

ensures that the intensity fluctuations due to target alignment are within ±10%.

This alignment procedure can be applied for transparent targets, e.g., thin plastic or diamond-like carbon (DLC) foils as well as opaque targets such as metal foils. The illumination of transparent targets is accomplished by transmitting the light from the LED through the target as shown in Figure 6(a). Therefore, the LED has to be installed inside the target chamber and is moved in and out of the diagnostics beamline using a motorized translation stage. For opaque targets the light from the LED is first collimated and then coupled into the diagnostics beamline with a beamsplitter cube outside the target chamber [Figure 6(b)]. Light which is reflected or scattered from the target is then detected by the CCD camera. The second method only works for a target thickness which is small compared to the Rayleigh range of the laser beam since the target surface that faces away from the laser is brought into the focal plane. For much thicker targets one could compensate for the (known) target thickness but this would introduce further inaccuracies and other alignment methods might be favored.

Examples for images of a micrometer thick plastic target and of the laser focus are given in Figures 7(a) and (b), respectively. The plastic foil was mounted on a supporting foil with a 1 mm aperture, which is partly visible in the image. The target itself is barely visible owing to little light scattered at its surface. For this reason micrometer-sized dust particles were applied onto the target surface during the manufacturing process and made focussing on the target surface possible.

5. Assessment and control of the on-target intensity

High-power CPA lasers can be classified into two different categories: pure Ti:sapphire systems that provide ultra-short pulses (<100 fs) with relatively low pulse energies (∼1 J) and systems that apply Nd:glass amplifiers to generate long pulses (∼500 fs) and high energies (>100 J). The presently achieved peak intensities are on the same order for both systems. While several theoretical models for the TNSA mechanism suggest that the maximum ion energies depend only on the laser intensity (e.g., Ref. [27]), much higher energies are typically achieved with the high energetic pulses from Nd:glass systems, even for similar intensities[28]. However, high-energy Nd:glass systems suffer from a poorer beam quality because of two reasons: first, the large size of the beam requires optics much more prone to manufacturing defects, and second, the lower thermal properties of glass induce large on-shot aberrations that are complicated to handle, even with adaptive optic techniques because of the low repetition rate of these systems. These aberrations reduce the accessible maximum intensity. Furthermore they add an additional uncertainty to the assessment of the on-target intensity which complicates the interpretation of experimental results. Novel acceleration mechanisms such as BOA or RPA are even more sensitive to variations of the intensity. According to the theoretical model of BOA this mechanism only works for a certain match of laser and target conditions[8]. For a given target material and thickness a certain intensity is required to achieve relativistic transparency. If the intensity is higher or lower than this optimum, transparency will set in too early or too late with respect to the impact of the pulse maximum and the mechanism will become ineffective. Hence, a well-defined on-target intensity which exceeds a certain limit (on the order of 10^{20} W cm^{-2} for BOA) is a mandatory precondition for the investigation of novel acceleration mechanisms.

At CPA systems the peak intensity of the fully amplified, compressed and focussed beam can be expressed as

$$I_{\max} = \frac{2 \cdot E_{\text{amp}} \cdot \eta_{\text{transp}} \cdot \eta_{\text{focus}} \cdot \eta_{\text{ab}}}{\Delta t \cdot \pi \cdot \omega_0^2}, \qquad (1)$$

with the duration of the compressed pulse Δt, the pulse energy after the last amplifier E_{amp}, the efficiency of the transport from the amplifier to the interaction chamber η_{transp}, the waist radius ω_0 and the energy fraction within the waist η_{focus}, both measured during alignment before the shot and a correction factor η_{ab} to account for degradation of the focus due to on-shot aberrations. Since there is no method to measure the on-shot intensity directly, all these quantities must be determined independently and the measurement errors of these parameters add up to the inaccuracy of the expected intensity.

For many experiments the typical way to estimate the on-shot intensity is to characterize the focal spot with a not fully amplified beam as described in Section 4 and assume a similar focus for the amplified beam. In this case the factor η_{ab} is not taken into account which leads to an overestimation of the intensity. This hinders the comparability of predictions by particle in cell simulations and experimental results and particularly leads to unrealistic expectations for the experimental outcome that could not be fulfilled in reality. In many cases the total uncertainty of the intensity is as high as one order of magnitude.

To show the influence of variations of the intensity on ion acceleration with submicrometer thick targets some typical

Table 1. Results from 2D particle in cell simulations. The TNSA maxima are the cutoff energies which are obtained with 1 μm thick plastic targets which stay opaque during the interaction. The BOA maxima are the cutoff energies obtained with the given optimum target thicknesses. Targets with these thicknesses are relativistically transparent when the pulse maximum impacts the target.

Intensity [10^{20} W cm^{-2}]	TNSA maxima [MeV]	BOA maximum [MeV]	Optimum target thicknesses [nm]
1	53	135	60
2	72	160	96
3	92	264	128

results obtained from 2D particle in cell simulations are given in Table 1. The simulation setup is identical to the one we described in Ref. [11]. Three different peak intensities from 1×10^{20} to 3×10^{20} W cm^{-2} are considered. Such a variation or ignorance of the experimental intensity by a factor of three is typical for many experiments. The TNSA maxima were obtained with 1 μm thick plastic targets which stayed opaque while interacting with the laser pulse for all three values of the intensity. The variation of the energy maxima for different intensities is in accordance with the well known square-root scaling for TNSA. For thinner targets relativistic transparency sets in leading to an enhanced acceleration. In this case the highest energy is obtained for an optimum match of laser intensity and target thickness. The optimum target thicknesses are also shown in Table 1. A variation of the intensity by a factor of three changes both the optimum target thickness and the maximum proton energy by about a factor of two. This example shows that the typical variations or uncertainties of the laser intensity could have an enormous effect on the results for ion acceleration with submicrometer thick targets and sufficient control of the intensity is a precondition for systematic studies.

At PHELIX, we have recently improved the quality of the fully amplified beam and the assessment of the intensity. On-shot aberrations are minimized by changing the lengths of two Kepler telescopes within the amplification chain from a configuration for the alignment mode to an on-shot configuration to compensate for defocus aberrations, a mirror after the main amplifier that is actively bent to compensate for astigmatism and a deformable mirror to minimize remaining aberrations. A detailed description of this technique will be published by Brabetz *et al.*[29]. The quality of the amplified beam is measured by using a Shack–Hartmann wavefront sensor and by mapping the far field after the main amplifier with a 16-bit CMOS camera (Hamamatsu model C11440-22CU). This enables an improved assessment of the on-shot intensity since the factor η_{ab} can now be included into the calculation. The pulse parameters of the PHELIX laser are summarized in Table 2. From these values an intensity of $(1.5 \pm 0.9) \times 10^{20}$ W cm^{-2} is calculated. For comparison, for the case were the bent mirror and the deformable mirror were not active and just the above-named lenses were used, a value of $\eta_{ab} = 0.1$–0.2 was measured for the aberrations resulting in an intensity on the order of only 5×10^{19} W cm^{-2}. Even though taking into account the factor η_{ab} improved the intensity estimate, the remaining uncertainty is still quite high. This becomes clear when one considers the influence of an intensity variation on the order of this uncertainty on the accelerated ions as summarized in Table 1. Therefore, the possibility to further improve the assessment of the intensity of the PHELIX system is currently investigated.

6. Results on ion acceleration with micrometer thick targets

With the above-named control of the temporal contrast, the focus and target alignment technique and the improved assessment of the intensity, investigation of ion acceleration with micrometer and submicrometer thick targets has become feasible at the PHELIX laser facility. A few experiments have been undertaken within the last 3 years of which the major results are published in Refs. [11, 30]. An example that shows the effect of the named improvements is given in Figure 8. It shows a selection of radiochromic film (RCF), which were exposed to the laser-accelerated proton beam from thin plastic targets. The RCF diagnostic was used in stack configuration as described in Ref. [31]. For the three cases (a) to (c) the laser pulse could be characterized by the first five parameters given in Table 2 but differed regarding the shot aberrations and the temporal contrast. For shot (a) a prepulse with a contrast ratio around 10^{-6} was present on the ns timescale, which originated from one of the regenerative amplifiers of the frontend. The imprint of the proton beam profile on the RCF features a ring-like structure with no intensity in the center. This could be explained by the destruction of the target by the prepulse in the center of the focus were the intensity is at maximum. Ion acceleration then only takes place from the non- or less disturbed part of the target around the wings of the focal spot. Due to the lower intensity in the interaction region only low maximum proton energies up to 28 MeV could be achieved. Shot (b) was undertaken after the prepulse had been removed by a new Pockels cell in the PHELIX frontend. The ring-like structure vanished and higher maximum proton energies up to 45 MeV were obtained. This result underlines the significance of a sufficiently high temporal contrast for ion acceleration with

Table 2. Pulse parameters of the PHELIX short pulse.

E_{amp}	Δt	ω_0	η_{transp}	η_{focus}	η_{ab}
(200 ± 10 J)	(750 ± 250 fs)	(3.7 ± 0.3 μm)	0.8 ± 0.1	0.25 ± 0.05	0.62 ± 0.24

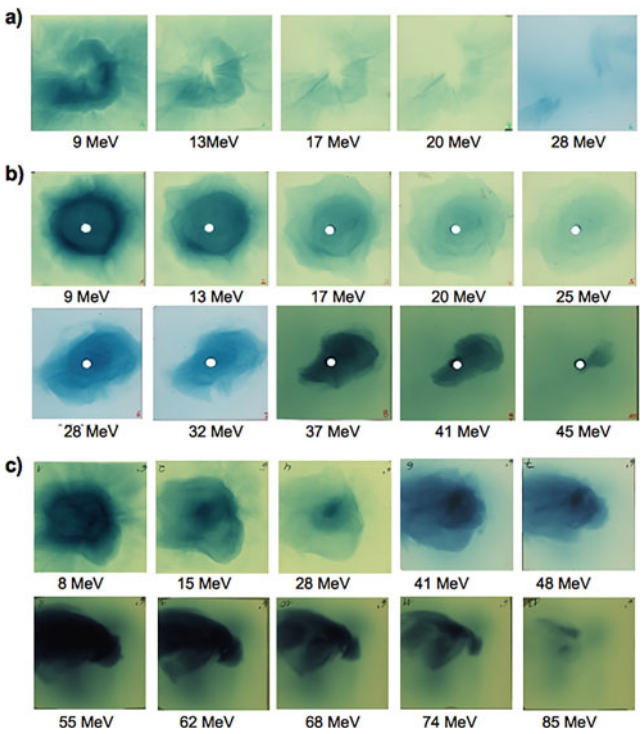

Figure 8. Selection of RCF which were exposed to laser-accelerated proton beams. The energy of protons which are fully stopped in the particular foil are written underneath each layer. Shown are examples for: (a) a shot with a ns-prepulse with a contrast ratio around 10^6, (b) a shot after removing the prepulse and (c) a shot using the full aberration control.

micrometer thick targets. For both shots (a) and (b) only the above-named lenses were used for aberration control leading to a reduced maximum intensity ($\sim 5 \times 10^{19}$ W cm^{-2}). With the full aberration control maximum proton energies up to 85 MeV were obtained which is a significant enhancement. As we showed in Ref. [11] such high maximum proton energies in excess of 70 MeV and particle numbers of 10^9 protons within an energy bin of 1 MeV around this maximum can be achieved in a very robust way by applying the TNSA mechanism and using target thicknesses around one micrometer.

7. Conclusion

To summarize, the improvement of the temporal contrast of the PHELIX pulse by applying a picosecond optical parametric amplifier to suppress the ASE and by exchanging components which generated prepulses, the use of micrometer and submicrometer thick targets has become feasible. Such targets are of particular interest for laser-ion acceleration studies. A novel focus and target alignment system has been implemented which enables positioning the target into the focal plane with an accuracy better than the Rayleigh range of the focussed beam. This minimizes intensity fluctuations from shot to shot due to target alignment. The focussed intensity of the PHELIX pulse has been increased by reducing on-shot aberrations. In addition the aberrations of the fully amplified beam are characterized and included into the calculation of the on-shot intensity. We showed that these improvements enabled maximum proton energies of up to 85 MeV for acceleration via the TNSA mechanism using submicrometer thick targets.

The investigation of alternative ion acceleration mechanisms such as BOA or RPA has become reachable. However, the effect of the slowly rising slope of the laser pulse on the 100 ps timescale on these mechanisms remains to be studied. One possibility to increase the contrast on this timescale is the combination of our contrast improving technique with one or two plasma mirrors.

Acknowledgments

This work has been partly funded by the EUROfusion Consortium (toIFE Programme, Grant Agreement No. 633053). The views and opinions expressed herein do not necessarily reflect those of the European Commission.

References

1. S. V. Bulanov and V. S. Khoroshkov, Plasma Phys. Rep. **28**, 453 (2002).
2. M. Roth, D. Jung, K. Falk, N. Guler, O. Deppert, M. Devlin, A. Favalli, J. Fernandez, D. Gautier, M. Geissel, R. Haight, C. E. Hamilton, B. M. Hegelich, R. P. Johnson, F. Merrill, G. Schaumann, K. Schoenberg, M. Schollmeier, T. Shimada, T. Taddeucci, J. L. Tybo, F. Wagner, S. A. Wender, C. H. Wilde, and G. A. Wurden, Phys. Rev. Lett. **110**, 044802 (2013).
3. M. Roth, T. E. Cowan, M. H. Key, S. P. Hatchett, C. Brown, W. Fountain, J. Johnson, D. M. Pennington, R. A. Snavely, S. C. Wilks, K. Yasuike, H. Ruhl, F. Pegoraro, S. V. Bulanov, E. M. Campbell, M. D. Perry, and H. Powell, Phys. Rev. Lett. **86**, 3 (2001).
4. R. A. Snavely, M. H. Key, S. P. Hatchett, T. E. Cowan, M. Roth, T. W. Phillips, M. A. Stoyer, E. A. Henry, T. C. Sangster, M. S. Singh, S. C. Wilks, A. MacKinnon, A. Offenberger, D. M. Pennington, K. Yasuike, A. B. Langdon, B. F. Lasinski, J. Johnson, M. D. Perry, and E. M. Campbell, Phys. Rev. Lett. **85**, 2945 (2000).
5. D. Neely, P. Foster, A. Robinson, F. Lindau, O. Lundh, A. Persson, C. G. Wahlström, and P. McKenna, Appl. Phys. Lett. **89**, 02150 (2006).
6. M. Kaluza, J. Schreiber, M. I. K. Santala, G. D. Tsakiris, K. Eidmann, J. Meyer-ter-Vehn, and K. J. Witte, Phys. Rev. Lett. **93**, 045003 (2004).
7. J. Fuchs, P. Antici, E. d'Humières, E. Lefebvre, M. Borghesi, E. Brambrink, C. A. Cecchetti, M. Kaluza, V. Malka, M. Manclossi, S. Meyroneinc, P. Mora, J. Schreiber, T. Toncian, H. Pépin, and P. Audebert, Nat. Phys. **2**, 4854 (2005).
8. L. Yin, B. J. Albright, B. M. Hegelich, K. J. Bowers, K. A. Flippo, T. J. T. Kwan, and J. C. Fernández, Phys. Plasmas **14**, 056706 (2007).

9. T. Esirkepov, M. Borghesi, S. V. Bulanov, G. Mourou, and T. Tajima, Phys. Rev. Lett. **92**, 175003 (2004).
10. V. Bagnoud, B. Aurand, A. Blazevic, S. Borneis, C. Bruske, B. Ecker, U. Eisenbarth, J. Fils, A. Frank, E. Gaul, S. Goette, C. Haefner, T. Hahn, K. Harres, H. M. Heuck, D. Hochhaus, D. H. H. Hoffmann, D. Javorková, H. J. Kluge, T. Kuehl, S. Kunzer, M. Kreutz, T. Merz-Mantwill, P. Neumayer, E. Onkels, D. Reemts, O. Rosmej, M. Roth, T. Stoehlker, A. Tauschwitz, B. Zielbauer, D. Zimmer, and K. Witte, Appl. Phys. B **100**, 137 (2010).
11. F. Wagner, O. Deppert, C. Brabetz, P. Fiala, A. Kleinschmidt, P. Poth, V. A. Schanz, A. Tebartz, B. Zielbauer, M. Roth, T. Stöhlker, and V. Bagnoud, Phys. Rev. Lett. **116**, 205002 (2016).
12. F. Wagner, S. Bedacht, A. Ortner, M. Roth, An. Tauschwitz, B. Zielbauer, and V. Bagnoud, Opt. Expr. **22**, 29505 (2014).
13. D. Batani, R. Jafer, M. Veltcheva, R. Dezulian, O. Lundh, F. Lindau, A. Persson, K. Osvay, C. G. Wahlström, D. C. Carroll, P. McKenna, A. Flacco, and V. Malka, New J. Phys. **12**, 045018 (2010).
14. D. Jung, L. Yin, B. J. Albright, D. C. Gautier, S. Letzring, B. Dromey, M. Yeung, R. Hörlein, R. Shah, S. Palaniyappan, K. Allinger, J. Schreiber, K. J. Bowers, H. C. Wu, J. C. Fernandez, D. Habs, and B. M. Hegelich, New J. Phys. **15** (2013).
15. F. Wagner, C. P. João, J. Fils, T. Gottschall, J. Hein, J. Körner, J. Limpert, M. Roth, T. Stöhlker, and V. Bagnoud, Appl. Phys. B **116**, 429 (2013).
16. M. Basko, J. Maruhn, and An. Tauschwitz, Development of a 2D radiation hydrodynamics code RALEF for laser plasma simulations, GSI report 2010-1, 410 (GSI Helmholtzzentrum für Schwerionenforschung GmbH, 2010).
17. J. Itatani, J. Faure, M. Nantel, G. Mourou, and S. Watanabe, Opt. Commun. **148**, 70 (1998).
18. M. P. Kalashnikov, E. Risse, H. Schönnagel, and W. Sandner, Opt. Lett. **30**, 923 (2005).
19. A. Jullien, O. Albert, F. Burgy, G. Hamoniaux, J.-P. Rousseau, J.-P. Chambaret, F. Augé-Rochereau, G. Chériaux, J. Etchepare, N. Minkovski, and S. M. Saltiel, Opt. Lett. **30**, 920 (2005).
20. K.-H. Hong, B. Hou, J. A. Nees, E. Power, and G. A. Mourou, Appl. Phys. B **81**, 447 (2005).
21. R. C. Shah, R. P. Johnson, T. Shimada, K. A. Flippo, J. C. Fernandez, and B. M. Hegelich, Opt. Lett. **34**, 2273 (2009).
22. C. Dorrer, I. A. Begishev, A. V. Okishev, and J. D. Zuegel, Opt. Lett. **32**, 2143 (2007).
23. C. P. João, F. Wagner, J. Körner, J. Hein, T. Gottschall, J. Limpert, and V. Bagnoud, Appl. Phys. B **118**, 401 (2015).
24. N. V. Didenko, A. V. Konyashchenko, A. P. Lutsenko, and S. Yu. Tenyakov, Opt. Express **16**, 3178 (2008).
25. F. Wagner, S. Bedacht, C. P. João, A. Ortner, M. Roth, T. Stöhlker, An. Tauschwitz, and V. Bagnoud, in *Proceedings of the 42nd EPS Conference on Plasma Physics, Contribution* P5.211 (2015).
26. V. A. Schanz, F. Wagner, M. Roth and V. Bagnoud are preparing a manuscript to be called *Enhanced Intensity Cross-correlator for High Energy Lasers (EICHEL) for contrast measurement at PHELIX laser facility*.
27. P. Mora, Phys. Rev. Lett. **90**, 185002 (2003).
28. H. Daido, M. Nishiuchi, and A. S. Pirozhkov, Rep. Prog. Phys. **75**, 056401 (2012).
29. C. Brabetz is preparing a manuscript to be called *Wavefront control at a high-energy, high-intensity laser*.
30. F. Wagner, S. Bedacht, V. Bagnoud, O. Deppert, S. Geschwind, R. Jaeger, A. Ortner, A. Tebartz, B. Zielbauer, D. H. H. Hoffmann, and M. Roth, Phys. Plasmas **22**, 063110 (2015).
31. F. Nürnberg, M. Schollmeier, E. Brambrink, A. Blazevic, D. C. Carroll, K. Flippo, D. C. Gautier, M. Geiel, K. Harres, B. M. Hegelich, O. Lundh, K. Markey, P. McKenna, D. Neely, J. Schreiber, and M. Roth, Rev. Sci. Instrum. **80**, 033301 (2009).